

Manuscript version: Author's Accepted Manuscript

The version presented in WRAP is the author's accepted manuscript and may differ from the published version or Version of Record.

Persistent WRAP URL:

<http://wrap.warwick.ac.uk/164796>

How to cite:

Please refer to published version for the most recent bibliographic citation information.

Copyright and reuse:

The Warwick Research Archive Portal (WRAP) makes this work by researchers of the University of Warwick available open access under the following conditions.

Copyright © and all moral rights to the version of the paper presented here belong to the individual author(s) and/or other copyright owners. To the extent reasonable and practicable the material made available in WRAP has been checked for eligibility before being made available.

Copies of full items can be used for personal research or study, educational, or not-for-profit purposes without prior permission or charge. Provided that the authors, title and full bibliographic details are credited, a hyperlink and/or URL is given for the original metadata page and the content is not changed in any way.

Publisher's statement:

Please refer to the repository item page, publisher's statement section, for further information.

For more information, please contact the WRAP Team at: wrap@warwick.ac.uk.

Long-Term Stability and Optoelectronic Performance Enhancement of InAsP Nanowires with an Ultra-Thin InP Passivation Layer

LuLu Chen,[†] Stephanie O. Adeyemo,[‡] H. Aruni Fonseka,[#] Huiyun Liu,[§] Srabani Kar,[‡] Hui Yang,^{//}* Anton Velichko,[¶] David J. Mowbray,[¶] Zhiyuan Cheng,[†] Ana M. Sanchez,[#] Hannah J Joyce,[‡]* Yunyan Zhang^{†§*}

[†] School of Micro-Nano Electronics, Zhejiang University, Hangzhou, Zhejiang, 311200, China

[‡] Electrical Engineering Division, Department of Engineering, University of Cambridge, 9 JJ Thomson Avenue, Cambridge CB3 0FA, United Kingdom;

[#] Department of Physics, University of Warwick, Coventry CV4 7AL, United Kingdom;

[§] Department of Electronic and Electrical Engineering, University College London, London WC1E 7JE, United Kingdom;

^{//} Institute for Materials Discovery, University College London, Roberts Building, Malet Place, London, WC1E 7JE, UK.

[¶] Department of Physics and Astronomy and the Photon Science Institute, University of Sheffield, Sheffield S3 7RH, U.K.

⊥ These authors contributed equally to the work.

Abstract: The influence of nanowire (NW) surface states increases rapidly with the reduction of diameter, and hence severely degrades the optoelectronic performance of narrow-diameter NWs. Surface passivation is therefore critical, but it is challenging to achieve long-term effective passivation without significantly affecting other qualities. Here, we demonstrate that an ultra-thin InP passivation layer of 2~3 nm can effectively solve the above challenges. On InAsP nanowires with small diameters of 30-40 nm, the ultra-thin passivation layer reduces the

surface recombination velocity by at least 70%, and increases the charge carrier lifetime by a factor of 3, and these improvements are maintained even after storing the samples in an ambient atmosphere for over 3 years. This passivation also greatly improves the performance thermal tolerance of these thin NWs, and extends their operating temperature from <150 K to room temperature. This study provides a new route towards high-performance room-temperature narrow-diameter NW devices with a long-term stability.

Key words: thin nanowire, surface passivation, ultra-thin InP, long-term stability, photonic properties

TOC graph:



Nanowires (NWs) feature a quasi-one-dimensional morphology and have many potential novel applications, including light emitters, photovoltaics, and high speed electronics.¹⁻⁵ They have significant advantages over thin-films/bulk III–V materials as they can be readily integrated on silicon (Si) substrates with high quality because their small contact area with the substrate confines the strain relaxation-formed dislocations to the vicinity of the NW/substrate interface. This means not only great flexibility in device design and potential for low-cost fabrication, but also seamless integration with the silicon industrial platform, solving the III–V/Si integration challenge that has been pursued for more than 40 years.^{6,7} Among different NWs, InAsP NWs have a narrow and direct band gap that can extend nanophotonic applications from near-infrared (~922 nm) to the mid-infrared spectral region (3.5 μm), and is an ideal material system for broadband photodetectors for applications in optical communications, surveillance, thermophotovoltaics and thermal imaging. It is also a good candidate to build high-efficiency light sources on Si, such as 1.3 μm and 1.5 μm lasers and single photon sources that will have important applications in Si photonics, quantum computing and quantum communication.

NWs have a large surface-to-volume ratio which can provide a greatly enlarged effective working area. For example, when used for photovoltaics, it can provide a junction area that is much larger than the cross section of NWs, which is beneficial for efficient carrier (electrons and holes) separation and collection.⁸ Unfortunately, the large surface-to-volume ratio of NWs also exacerbates the influence of surface states that can cause severe Fermi-level pinning, depletion of charge carriers, increased charge carrier scattering and high non-radiative surface recombination rates, leading to slow device response and low efficiency.^{9,10} The influence of the surface states increases rapidly with the surface-to-volume ratio when the NW diameter reduces. The surface states can even deplete the whole volume of thin NWs, rendering them unusable for devices.^{11,12} Furthermore, III-V materials, especially high-InAs-content ones with a small band gap, have small charge carrier effective masses and hence high charge carrier

mobilities, so carriers easily reach the NW surface.¹³ With increasing operating temperature, surface traps become activated, leading to severe charge carrier loss. As we will show below, this is one of the main reasons that un-passivated (bare) thin NWs only have good optoelectronic performance at low temperature, which presents a challenge towards achieving high quantum efficiency at room temperature, and hinders the development of room-temperature high-performance optoelectronic and photonic devices. Due to these reasons, most studies of high-InAs-content NWs so far have been primarily focused on the fabrication of electronic devices,¹⁴⁻¹⁶ while the optoelectronic niche remains largely understudied, especially for NWs with smaller diameters.

Surface passivation is thus critical for InAsP thin-NW devices to achieve high performance, but at this stage there is still a lack of an effective and stable passivation method. Chemical passivation, such as with sulphide solutions, can provide an effective instant passivation, which however lacks long-term stability.^{17,18} A more effective and robust passivation technique is using in-situ-grown inorganic materials with a wider band gap that can block carriers from reaching the surface states. However, to achieve effective passivation, a passivation layer with a thickness in the order of 10-100 nm is required to prevent carrier tunnelling to the surface, which puts high requirements on lattice matching between the NWs and the passivation layers. Thus, the most widely used surface passivation methods for GaAs-based NWs utilize closely lattice-matched shells of a different material, including AlGaAs,¹⁹⁻²¹ AlInP,²² and InGaP.²³ With the exception of GaAs/AlGaAs, achieving a lattice-matched shell composition requires careful tuning of growth parameters for each individual system. This is particularly challenging for NW growth owing to the different diffusion lengths of different adatoms on the substrate and nanowire surface, which can give rise to non-uniform composition both within and between different nanowires.²⁴ For InAsP NWs, Al(Ga)AsSb is lattice matched but suffers a wide miscibility gap which makes growing the required alloy compositions extremely

challenging. The use of a thick lattice-mismatched material will introduce large strain and seriously degrade the crystal quality.²⁵ The strain induced by a thicker lattice-mismatched shell inevitably affects the band structure and NW morphology, limiting further device possibilities. Therefore, an alternative passivation method will be needed for InAsP NWs that requires no lattice-matching and has little impact on the other properties.

An alternative passivation route is to overcoat the NW with a material that itself has a low surface recombination velocity, so that recombination is reduced even when substantial tunnelling into the layer occurs. Among the III-V materials, InP has an ultra-low surface recombination velocity of ~ 170 cm/s that is much lower than other III-Vs (e.g. GaAs = $\sim 5.4 \times 10^5$ cm/s).¹⁰ InP-based materials thus have been used widely for surface passivation.²⁶⁻²⁸ For example, Holm *et al.* covered their GaAsP NW solar cell with an additional shell of ~ 10 nm InGaP, and improved the efficiency from $\sim 6\%$ to $>10\%$.²⁹ Considering the passivating nature of InP material, it is highly likely that even an ultra-thin layer of InP of a few nm can still have a substantial passivation effect, which may obviate the need for a thick passivation layer and hence circumvent the lattice-matching issue. This idea has been proved to be highly effective in improving the carrier mobility of InAs-based transistors by solving the surface-band bending issue, and reducing the surface roughness and detrimental effect of ionized impurity scattering centers.³⁰⁻³² However, the performance of an electronic device relies only on the dynamics of one type of injected carrier (either electrons or holes); whereas optoelectronic performance is controlled by the complex interaction between both types of carriers. Optoelectronic performance therefore requires dedicated study beyond electronic studies alone. In addition, the long-term stability is critical for the lifetime of NW-based devices. So far, there is still a lack of detailed and systematic reports on whether the ultra-thin InP layer can provide long-term protection to the optical and optoelectronic properties of passivated InAs-based NWs.

In this study, the long-term passivation effect of using ultra-thin InP cladding layer is investigated on InAsP NWs of a small diameter (30 ~ 40 nm). Even after storing in an ambient atmosphere for over 3 years, this passivation technique can still effectively reduce the surface recombination rate, and enhance the carrier lifetime, leading to greatly improved optical properties with largely enhanced thermal stability.

The InAs_{0.8}P_{0.2} NWs were grown by molecular beam epitaxy (MBE) without using foreign-metal catalysts. The majority of the NWs are standing vertically on the silicon substrate with a very thin diameter of 30 ~ 40nm and a length of ~500 nm (Figure 1a). After cladding with a thin layer of InP, the NWs are slightly bent due to the introduction of strain (Figure 1b). The morphology and compositional analysis of the InAsP/InP was further analysed using STEM along the <112> direction. Phosphorous maps and elemental distribution profiles in the radial direction of NW reveal a thin P-rich shell 2~3 nm in thickness (Figure 1c and d), corroborated by the intensity profile taken in the NW radial direction in <112>-Annular Dark Field images in Figure 1f. The InP shell was grown at an extremely low growth rate of 0.077ML/S which is far lower than normal growth rate of 1ML/S. So, a uniform shell is expected. However, it may be affected by the shadowing effect of the neighbouring NWs. So, the InP shell thickness was measured at the tip of NWs to identify the biggest thickness of the entire NW. Further optimization may be performed by using patterned substrates to allow accurate control of the inter-wire distance.³³ The crystal structure was determined using images of NWs along <110> (Figure 1e). Higher magnification images of areas similar to the one enclosed in the red square confirmed the presence of stacking faults, with a mixture of wurtzite (WZ) and zincblende (ZB) phases, similar to previous reports.^{34,35} . No dislocations were observed due to the small InP thickness (Figure 1g).

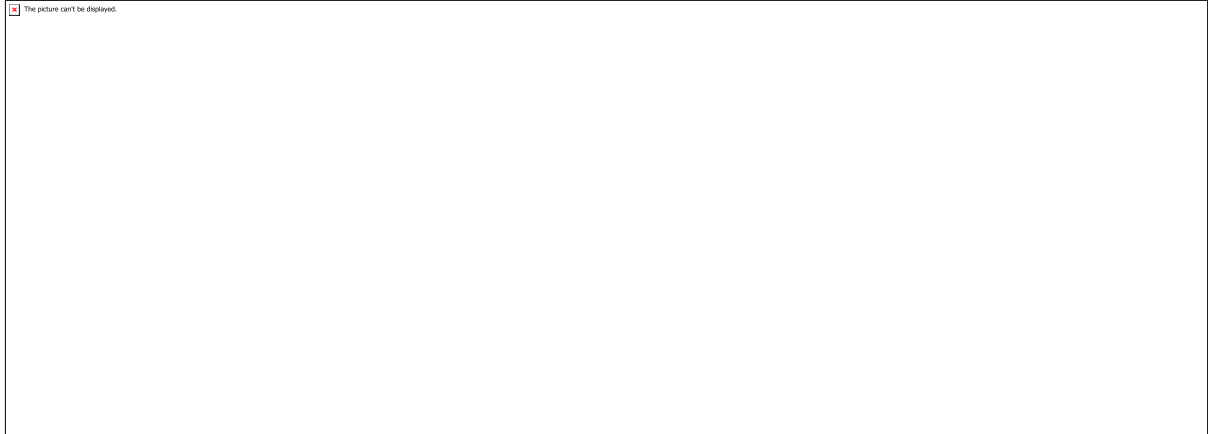


Figure 1. Morphology of InAsP NWs with and without InP passivation. (a) Bare InAsP NWs. (b) InAsP NWs cladded by ~ 3 nm InP. (c)-(g) are measurement results from NWs in (b). (c) P map and (d) elemental distribution in a NW segment, confirming a P-rich shell. (e) ADF along $\langle 110 \rangle$ of a nanowire. (f) ADF-STEM image along $\langle 112 \rangle$ direction revealing the NW shape with a shell thickness ~ 2 -3 nm. (g) Atomically resolved $\langle 110 \rangle$ ADF-STEM image of NW area enclosed in the red square in figure (e).

After being stored in an ambient atmosphere for over 3 years, optical pump–terahertz probe spectroscopy (OPTP) was performed to probe bare and passivated InAsP nanowires to study the influence of the ultra-thin InP surface passivation layer on the dynamics of the photogenerated carriers. The bare and passivated nanowires were placed on individual quartz substrates and were photoexcited with an optical pump pulse centred at 2060 nm (0.6 eV) just above the bandgap of the InAsP core. This excitation energy selectively photoexcites the core, but not the InP shells. This allows the effective comparison of the charge carrier dynamics of the passivated and unpassivated nanowires. The photoexcitation pulse induced a change in the transmission of the terahertz (THz) probe pulse, ΔE . The measured ΔE is directly proportional to the photoconductivity change ($\Delta\sigma$) of the nanowires.

The room-temperature photoconductivity ($\Delta\sigma$) decays obtained from the OPTP measurements on InAsP and InAsP/InP nanowires are presented in Figure 2a. The $\Delta\sigma$ decays shows that the passivated nanowires have slower recombination in contrast to the rapid $\Delta\sigma$ decay of the bare

InAsP nanowires. This comparison suggests that surface traps are responsible for the rapid $\Delta\sigma$ decay of bare InAsP nanowires and that these traps were effectively reduced by passivating with a thin InP layer. The $\Delta\sigma$ decay of the bare InAsP nanowires is well-fitted by a monoexponential function, which is further evidence that charge carriers recombine rapidly through trap-assisted Shockley–Read–Hall mechanisms. The $\Delta\sigma$ decay of the passivated InAsP/InP nanowires deviates from a monoexponential function and slows with time after photoexcitation, indicating that the remaining traps may saturate as they are filled. The photoconductivity decays were fitted at early times after photoexcitation to assess the surface recombination rate when the surface traps are originally unoccupied. The decays were fitted with monoexponential functions yielding charge carrier lifetimes τ of ~ 120 ps for the bare InAsP nanowires and ~ 340 ps for the passivated nanowires corresponding to an increase in the carrier lifetime by a factor of ~ 3 . This highlights the effectiveness of the ultra-thin passivation layer in reducing surface state density in the InAsP nanowires. The effective recombination time in nanowires is closely approximated by

$$\frac{1}{\tau} = \frac{1}{\tau_{volume}} + \frac{4S}{d} \quad (1)$$

where d is the nanowire diameter, S is the surface recombination velocity and τ_{volume} is the time constant for recombination within the nanowire's volume. By fitting equation (1) to the experimental charge carrier lifetime τ values, and assuming τ_{volume} is the same for passivated and unpassivated nanowires, we calculate that the InP surface passivation lowers the surface recombination velocity in the InAsP nanowires by $\Delta S = 6.1 \times 10^3$ cm/s compared to the bare InAsP nanowires thereby allowing an increase in the fraction of radiative recombination in the InAsP nanowires. To estimate the surface recombination velocity in the passivated nanowires, $S_{InAsP/InP} = S_{InAsP} - \Delta S$, we consider ΔS and the surface recombination velocity in unpassivated nanowires, S_{InAsP} . As the composition of the unpassivated InAsP nanowires is

close to that of InAs nanowires, it is expected that the surface recombination velocity S value should be close to or less than that of InAs nanowires, which we measure to be $S_{\text{InAs}} = 8.7 \times 10^3$ cm/s (Supporting Information Figure S1) consistent with previous reports.¹⁰ Assuming $S_{\text{InAsP}} \lesssim S_{\text{InAs}} = 8.7 \times 10^3$ cm/s and ΔS of 6.1×10^3 cm/s, an approximate upper limit of $S_{\text{InAsP/InP}} = 2.6 \times 10^3$ cm/s is extracted for the passivated InAsP/InP nanowires. The increase in charge carrier lifetime and decreased surface recombination velocity indicates a large reduction in the surface states density by the highly effective ultra-thin InP shell.

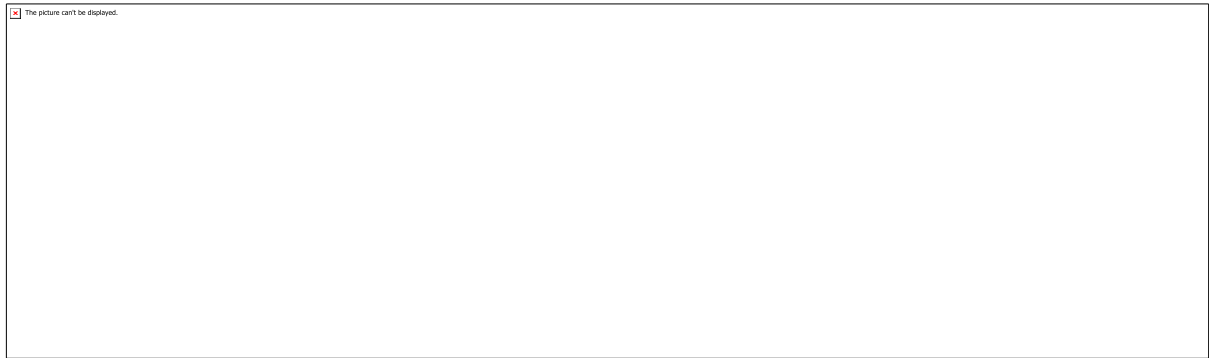


Figure 2. Influence of the InP surface passivation layer on carrier dynamics. (a) Normalised photoconductivity decays of InAsP and InAsP/InP nanowires on a semilogarithmic scale. The lines are monoexponential fits to the decay. Photoconductivity spectra of (b) InAsP and (c) InAsP/InP nanowires at a time delay of 10 ps after photoexcitation. Dots represent data points and black solid lines are Lorentzian fits.

The photoconductivity spectra of both nanowire samples shown in Figures 2b and 2c were measured at 10 ps after photoexcitation and each spectrum was fitted with a Lorentzian function:

$$\sigma(\omega) = \frac{Ne^2}{m^*} \frac{i\omega}{\omega^2 - \omega_0^2 - i\omega\gamma} \quad (2)$$

This Lorentzian response is typical of plasmon modes of semiconductor nanostructures. For the effective mass m_e^* , we use the value for bulk InAsP semiconductors namely $m_e^* = 0.0347m_e$.³⁶ The measured photoconductivity $\Delta\sigma$ is predominantly from electrons since the

effective hole mass in InAs is significantly larger than that of the electrons. From the fitting, the carrier scattering rates and electron mobilities are extracted. The extracted carrier mobilities are $\sim 3200 \text{ cm}^2\text{V}^{-1}\text{s}^{-1}$ for both the passivated nanowires and the bare InAsP nanowires, thus showing that there is no significant degradation in mobility caused by lattice mismatch-induced strain between the core and the shell. Previous field-effect transistor (FET) measurements on InAs nanowires have reported increases in transconductance with InP passivation, attributed to the reduction of the electron accumulation layer at the surface (see reference 32). It should be noted that unlike FET measurements, our OPTP measurements of mobility do not require approximations of the gate oxide capacitance, and are therefore free of any systematic errors in mobility that can be introduced by this term. In the present study, regardless of passivation, the measured mobilities are an order of magnitude lower than those of bulk InAs ($40,000 \text{ cm}^2\text{V}^{-1}\text{s}^{-1}$) which may be due to the presence of stacking faults in these NW structures.³⁷ Compositional fluctuations in the axial direction are also possible, which may cause additional carrier scattering.³⁸

The power-dependent performance of the InAsP NWs with and without surface passivation was then studied by photoluminescence (PL) measurements. The power-dependent PL spectra obtained at 12 K are shown in Figure 3a and b. The unpassivated NWs exhibit a broad PL spectrum peaking between 2400 and 2600 nm (0.48 to 0.52 eV). In contrast, the InP-passivated NWs (Figure 1b) exhibit a blue-shifted peak centred at 2200 nm (0.56 eV) due to strain caused by the InP passivation, which is in accordance with the slight NW bending.^{39, 40} As can be seen in Figure 3a and 3c, the PL intensity of the bare NWs increases with excitation power at low excitation power range, but saturates and then decreases rapidly above 600 mW. This saturation is attributed to laser excitation-induced wire heating which activates surface traps to increase non-radiative recombination. At low excitation powers, the wire laser-heating effect is small, the diffusion of the carriers is slow and hence a larger fraction of carriers recombine

radiatively inside the NWs, which allows the emission intensity to increase with the excitation power. At high excitation powers, the wire is heated to higher temperatures and enhanced carrier diffusion drives them to the surface, where they are captured by the high-density surface traps to reduce radiative recombination efficiency. Thus, the non-radiative carrier loss increases severely and hence the emission intensity reduces with the increase of the excitation power. After the surface passivation, the carrier loss is greatly reduced and the NWs do not show the phenomenon of reduced PL intensity at high excitation powers, which can be seen in Figure 3b and c.

The power-dependent performance of the bare NWs changes significantly with temperature. As can be seen in the low excitation power region in Figure 3d, the integrated emission intensity increases rapidly with the excitation power at 12 K; while the increase is much slower at 110 K and the intensity is one order of magnitude lower. This suggests that the increased temperature and hence thermal energy is enough to cause severe charge carrier loss at the surface. In contrast, the passivated NWs show almost similar power-dependent performance from low temperature to room temperature, and their emission intensity at room temperature is stronger than that of the bare NWs at 12 K. With the increase in temperature, the emission intensity ratio between the bare and passivated NWs increases almost linearly, which can be seen in Figure 3e. The passivated NWs can still show strong emission at room temperature, while the emission of bare NWs is below our system detection limit for temperatures above 150 K (Figure 3f). All these further suggest that the surface passivation by thin InP can greatly improve the optoelectronic performance of the NWs at high temperatures and high carrier densities, which is highly important for practical applications of narrow-band-gap semiconductor NWs.

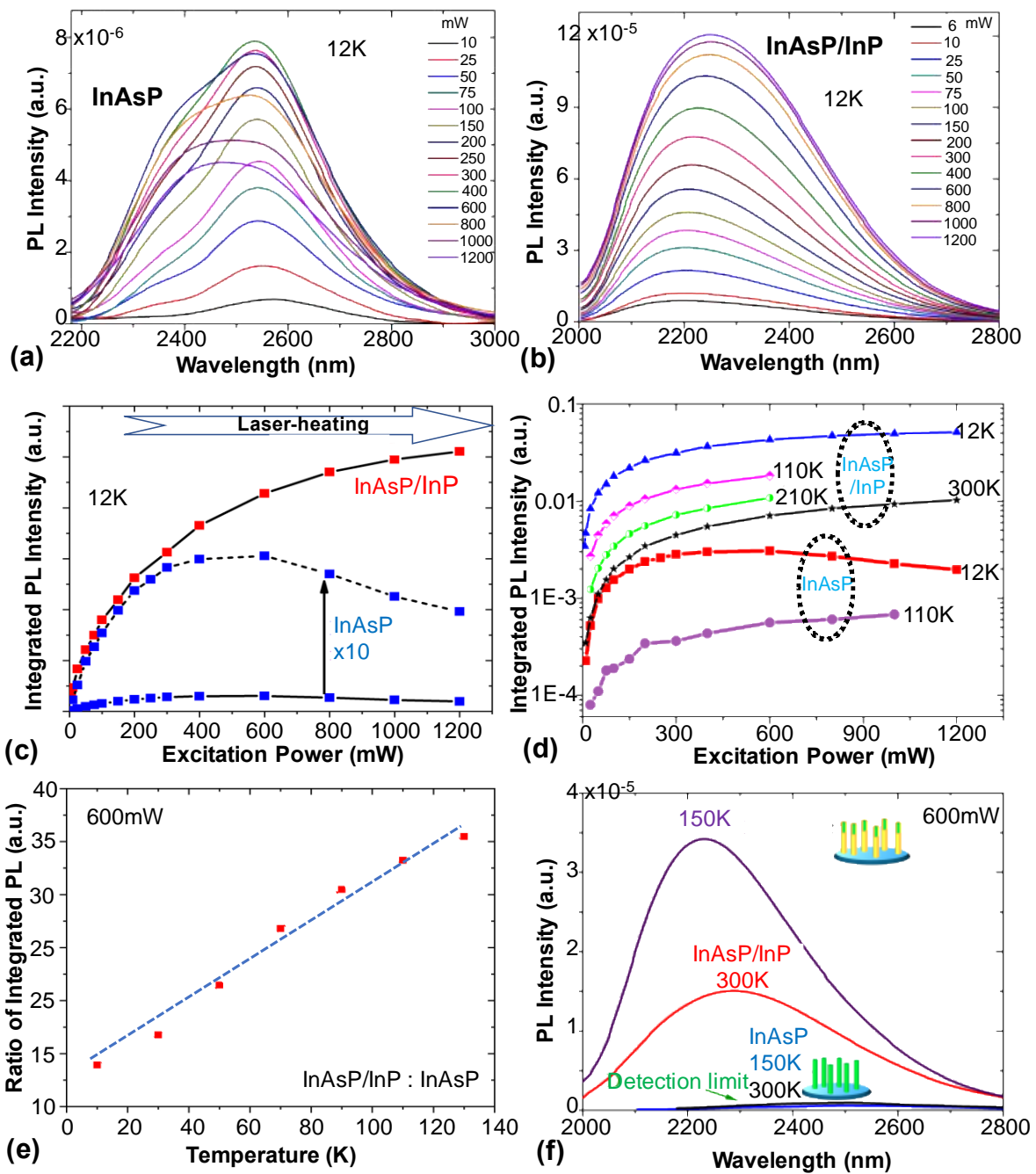


Figure 3. Thermal tolerance of InAsP NWs with and without surface passivation. (a) and (b) are the power-dependent PL spectra of InAsP and InAsP/InP NWs at 12K, respectively. (c) Integrated PL intensity as a function of excitation power at (c) 12K and (d) different temperatures. (e) Integrated PL intensity ratio between passivated and bare NWs (InAsP/InP/InAsP) as a function of temperature at 600mW excitation power. (f) PL spectra of both samples measured at 150K and 300K.

In conclusion, thin InAsP NWs (30 ~ 40 nm diameter) without surface passivation are highly

sensitive to the thermal environment and their performance degrades rapidly with temperature, making their PL emission quench at ~ 150 K and preventing their room temperature applications. An ultra-thin InP layer ($2 \sim 3$ nm) with good surface properties, e.g. low surface state density, can be used to passivate the NW surface, and its effectiveness and long-term stability have been investigated systematically after these samples have been stored in atmosphere for over 3 years. The InP passivation layer does not have any observable defects despite the large lattice mismatch with the core NWs due to being very thin. Upon passivation, the density of surface states dramatically decreased by at least 70%, and the lifetime and mobility of the carriers increased by a factor of ~ 3 . These improvements lead to greatly enhanced temperature/thermal stability, and significantly expands the maximum operating temperature from ~ 130 K to room-temperature. With this efficient passivation technique, the performance of the NWs at room temperature is superior to that of the bare NWs at 12 K. This study provides an effective and long-term passivation method for narrow-band-gap semiconductor NWs to realize high-temperature performance.

Methods:

NW growth: The InAsP NWs were grown directly on Si substrates by solid-source III–V molecular beam epitaxy without using foreign catalytic metals. The core InAsP NWs were grown with an In beam equivalent pressure, V/III flux ratio, P/(As+P) flux ratio, and substrate temperature of 2.75×10^{-8} Torr, ~ 200 , 60%, and ~ 455 °C, respectively. The passivation InP shells were then grown with an In beam equivalent pressure, V/III flux ratio, and substrate temperature of 2.75×10^{-8} Torr, ~ 90 , and ~ 400 °C, respectively. The substrate temperature was measured by a pyrometer. The low temperature for shell growth is for achieving uniform shells. The NW sidewall is normally $\{110\}$ which has very low surface energy. Ad-atoms are much more mobile on this surface than on the commonly used $\{100\}$ facets. Therefore, a low

temperature is necessary to reduce the mobility of ad-atoms and enhance their nucleation ability.⁴¹

Scanning Electron Microscope (SEM): The NW morphology was measured with a Zeiss XB 1540 FIB/SEM system.

Transmission electron microscopy (TEM): Simple scraping of the NWs onto a lacey carbon support was used to prepare TEM specimens. The TEM measurements were performed with a JEOL 2100 and doubly-corrected ARM200F microscopes, both operating at 200 kV.

Optical pump-terahertz probe spectroscopy (OPTP): An amplified Ti:Sapphire laser with 8 W average power was used to generate 35 fs pulses centred at 800 nm. The optical alignment follows that described in Ref. 42 for OPTP spectroscopy. THz pulses were generated by optical rectification in a ZnTe (110) crystal. The nanowire sample was photoexcited by an optical pump pulse centred at 2060 nm (0.6 eV). The electric field of the THz pulse transmitted through the sample was detected by electro-optic sampling using a ZnTe (110) crystal and a balanced photodiode circuit.

Photoluminescence (PL): A mid-IR PL setup has been used to analyze the photoluminescence properties of both samples. A 532 nm laser was used to illuminate the samples and a liquid nitrogen cooled InSb detector to record the photoluminescence of the samples.

Author Information

Corresponding Author: Yunyan Zhang

Email: yunyanzhang@zju.edu.cn

Notes:

The authors declare no competing financial interest.

Acknowledgements:

The authors acknowledge the support of the Leverhulme Trust, the EPSRC (grant nos. EP/P000916/1, EP/P000886/1, EP/P006973/1), the European Research Council (ERC Starting Grant no. 716471, ACrossWire) and the EPSRC National Epitaxy Facility. S.O.A thanks the EPSRC for her International Doctoral Studentship.

Supporting Information:

Photoconductivity decay data for unpassivated InAs nanowires. This material is available free of charge via the internet at <http://pubs.acs.org>.

References:

-
- (1) Lieber, C. M.; Wang, Z. L. Functional Nanowires. *MRS Bulletin* **2007**, 32 (2), 99–108.
<https://doi.org/10.1557/mrs2007.41>.
 - (2) Zhang, Y.; Wu, J.; Aagesen, M.; Liu, H. III–V Nanowires and Nanowire Optoelectronic Devices. *Journal of Physics D: Applied Physics* **2015**, 48 (46), 463001.
<https://doi.org/10.1088/0022-3727/48/46/463001>
 - (3) Yan, R.; Gargas, D.; Yang, P. Nanowire Photonics. *Nature Photon* **2009**, 3 (10), 569–576.
<https://doi.org/10.1038/nphoton.2009.184>.
 - (4) Dasgupta, N. P.; Sun, J.; Liu, C.; Brittman, S.; Andrews, S. C.; Lim, J.; Gao, H.; Yan, R.; Yang, P. 25th Anniversary Article: Semiconductor Nanowires – Synthesis, Characterization, and Applications. *Advanced Materials* **2014**, 26 (14), 2137–2184.
<https://doi.org/10.1002/adma.201305929>.
 - (5) Yang, P.; Yan, R.; Fardy, M. Semiconductor Nanowire: What’s Next? *Nano Lett.* **2010**, 10 (5), 1529–1536.
<https://doi.org/10.1021/nl100665r>.
 - (6) Roelkens, G.; Liu, L.; Liang, D.; Jones, R.; Fang, A.; Koch, B.; Bowers, J. III-V/Silicon Photonics for on-Chip and Intra-Chip Optical Interconnects. *Laser & Photonics Reviews* **2010**, 4 (6), 751–779.
<https://doi.org/10.1002/lpor.200900033>.
 - (7) Mathine, D. L. The Integration of III-V Optoelectronics with Silicon Circuitry. *IEEE Journal of Selected Topics in Quantum Electronics* **1997**, 3 (3), 952–959.
<https://doi.org/10.1109/2944.640649>.

-
- (8) Krogstrup, P.; Jørgensen, H. I.; Heiss, M.; Demichel, O.; Holm, J. V.; Aagesen, M.; Nygard, J.; Fontcuberta i Morral, A. Single-Nanowire Solar Cells beyond the Shockley–Queisser Limit. *Nature Photon* **2013**, *7* (4), 306–310.
<https://doi.org/10.1038/nphoton.2013.32>.
- (9) Joyce, H. J.; Baig, S. A.; Parkinson, P.; Davies, C. L.; Boland, J. L.; Tan, H. H.; Jagadish, C.; Herz, L. M.; Johnston, M. B. The Influence of Surfaces on the Transient Terahertz Conductivity and Electron Mobility of GaAs Nanowires. *J. Phys. D: Appl. Phys.* **2017**, *50* (22), 224001.
<https://doi.org/10.1088/1361-6463/aa6a8f>.
- (10) Joyce, H. J.; Docherty, C. J.; Gao, Q.; Tan, H. H.; Jagadish, C.; Lloyd-Hughes, J.; Herz, L. M.; Johnston, M. B. Electronic Properties of GaAs, InAs and InP Nanowires Studied by Terahertz Spectroscopy. *Nanotechnology* **2013**, *24* (21), 214006.
<https://doi.org/10.1088/0957-4484/24/21/214006>.
- (11) Chang, C.-C.; Chi, C.-Y.; Yao, M.; Huang, N.; Chen, C.-C.; Theiss, J.; Bushmaker, A. W.; LaLumondiere, S.; Yeh, T.-W.; Povinelli, M. L.; Zhou, C.; Dapkus, P. D.; Cronin, S. B. Electrical and Optical Characterization of Surface Passivation in GaAs Nanowires. *Nano Lett.* **2012**, *12* (9), 4484–4489.
<https://doi.org/10.1021/nl301391h>.
- (12) Demichel, O.; Heiss, M.; Bleuse, J.; Mariette, H.; Fontcuberta i Morral, A. Impact of Surfaces on the Optical Properties of GaAs Nanowires. *Appl. Phys. Lett.* **2010**, *97* (20), 201907. <https://doi.org/10.1063/1.3519980>.
- (13) Metzger, W. K.; Wanlass, M. W.; Gedvilas, L. M.; Verley, J. C.; Carapella, J. J.; Ahrenkiel, R. K. Effective Electron Mass and Plasma Filter Characterization of N-Type InGaAs and InAsP. *Journal of Applied Physics* **2002**, *92* (7), 3524–3529.
<https://doi.org/10.1063/1.1504170>.
- (14) Wei, W.; Bao, X.-Y.; Soci, C.; Ding, Y.; Wang, Z.-L.; Wang, D. Direct Heteroepitaxy of Vertical InAs Nanowires on Si Substrates for Broad Band Photovoltaics and Photodetection. *Nano Lett.* **2009**, *9* (8), 2926–2934.
<https://doi.org/10.1021/nl901270n>.
- (15) Ford, A. C.; Ho, J. C.; Chueh, Y.-L.; Tseng, Y.-C.; Fan, Z.; Guo, J.; Bokor, J.; Javey, A. Diameter-Dependent Electron Mobility of InAs Nanowires. *Nano Lett.* **2009**, *9* (1), 360–

<https://doi.org/10.1021/nl803154m>.

- (16) Tanaka, T.; Tomioka, K.; Hara, S.; Motohisa, J.; Sano, E.; Fukui, T. Vertical Surrounding Gate Transistors Using Single InAs Nanowires Grown on Si Substrates. *Appl. Phys. Express* **2010**, *3* (2), 025003.
<https://doi.org/10.1143/APEX.3.025003>.
- (17) Tajik, N.; Peng, Z.; Kuyanov, P.; LaPierre, R. R. Sulfur Passivation and Contact Methods for GaAs Nanowire Solar Cells. *Nanotechnology* **2011**, *22* (22), 225402.
<https://doi.org/10.1088/0957-4484/22/22/225402>.
- (18) Petrovykh, D. Y.; Yang, M. J.; Whitman, L. J. Chemical and Electronic Properties of Sulfur-Passivated InAs Surfaces. *Surface Science* **2003**, *523* (3), 231–240.
[https://doi.org/10.1016/S0039-6028\(02\)02411-1](https://doi.org/10.1016/S0039-6028(02)02411-1).
- (19) Joyce, H. J.; Parkinson, P.; Jiang, N.; Docherty, C. J.; Gao, Q.; Tan, H. H.; Jagadish, C.; Herz, L. M.; Johnston, M. B. Electron Mobilities Approaching Bulk Limits in “Surface-Free” GaAs Nanowires. *Nano Lett.* **2014**, *14* (10), 5989–5994.
<https://doi.org/10.1021/nl503043p>.
- (20) Titova, L. V.; Hoang, T. B.; Jackson, H. E.; Smith, L. M.; Yarrison-Rice, J. M.; Kim, Y.; Joyce, H. J.; Tan, H. H.; Jagadish, C. Temperature Dependence of Photoluminescence from Single Core-Shell GaAs–AlGaAs Nanowires. *Appl. Phys. Lett.* **2006**, *89* (17), 173126.
<https://doi.org/10.1063/1.2364885>.
- (21) Hoang, T. B.; Titova, L. V.; Yarrison-Rice, J. M.; Jackson, H. E.; Govorov, A. O.; Kim, Y.; Joyce, H. J.; Tan, H. H.; Jagadish, C.; Smith, L. M. Resonant Excitation and Imaging of Nonequilibrium Exciton Spins in Single Core–Shell GaAs–AlGaAs Nanowires. *Nano Lett.* **2007**, *7* (3), 588–595.
<https://doi.org/10.1021/nl062383q>.
- (22) Chia, A. C. E.; Tirado, M.; Li, Y.; Zhao, S.; Mi, Z.; Comedi, D.; LaPierre, R. R. Electrical Transport and Optical Model of GaAs–AlInP Core-Shell Nanowires. *Journal of Applied Physics* **2012**, *111* (9), 094319.
<https://doi.org/10.1063/1.4716011>.
- (23) Sköld, N.; Karlsson, L. S.; Larsson, M. W.; Pistol, M.-E.; Seifert, W.; Trägårdh, J.; Samuelson, L. Growth and Optical Properties of Strained GaAs–GaxIn1-XP Core–Shell

-
- Nanowires. *Nano Lett.* **2005**, *5* (10), 1943–1947.
<https://doi.org/10.1021/nl051304s>.
- (24) Kim, Y.; Joyce, H. J.; Gao, Q.; Tan, H. H.; Jagadish, C.; Paladugu, M.; Zou, J.; Suvorova, A. A. Influence of Nanowire Density on the Shape and Optical Properties of Ternary InGaAs Nanowires. *Nano Lett.* **2006**, *6* (4), 599–604.
<https://doi.org/10.1021/nl052189o>.
- (25) Treu, J.; Bormann, M.; Schmeiduch, H.; Döblinger, M.; Morkötter, S.; Matich, S.; Wiecha, P.; Saller, K.; Mayer, B.; Bichler, M.; Amann, M.-C.; Finley, J. J.; Abstreiter, G.; Koblmüller, G. Enhanced Luminescence Properties of InAs–InAsP Core–Shell Nanowires. *Nano Lett.* **2013**, *13* (12), 6070–6077.
<https://doi.org/10.1021/nl403341x>.
- (26) Jurczak, P.; Zhang, Y.; Wu, J.; Sanchez, A. M.; Aagesen, M.; Liu, H. Ten-Fold Enhancement of InAs Nanowire Photoluminescence Emission with an InP Passivation Layer. *Nano Lett.* **2017**, *17* (6), 3629–3633.
<https://doi.org/10.1021/acs.nanolett.7b00803>.
- (27) Haggren, T.; Jiang, H.; Kakko, J.-P.; Huhtio, T.; Dhaka, V.; Kauppinen, E.; Lipsanen, H. Strong Surface Passivation of GaAs Nanowires with Ultrathin InP and GaP Capping Layers. *Appl. Phys. Lett.* **2014**, *105* (3), 033114.
<https://doi.org/10.1063/1.4891535>.
- (28) Mariani, G.; Scofield, A. C.; Hung, C.-H.; Huffaker, D. L. GaAs Nanopillar-Array Solar Cells Employing in Situ Surface Passivation. *Nat Commun* **2013**, *4* (1), 1497.
<https://doi.org/10.1038/ncomms2509>.
- (29) Holm, J. V.; Jørgensen, H. I.; Krogstrup, P.; Nygård, J.; Liu, H.; Aagesen, M. Surface-Passivated GaAsP Single-Nanowire Solar Cells Exceeding 10% Efficiency Grown on Silicon. *Nat Commun* **2013**, *4* (1), 1498.
<https://doi.org/10.1038/ncomms2510>.
- (30) Liu, X.; Liu, P.; Huang, H.; Chen, C.; Jin, T.; Zhang, Y.; Huang, X.; Jin, Z.; Li, X.; Tang, Z. Growth and Large-Scale Assembly of InAs/InP Core/Shell Nanowire: Effect of Shell Thickness on Electrical Characteristics. *Nanotechnology* **2013**, *24* (24), 245306.
<https://doi.org/10.1088/0957-4484/24/24/245306>.

-
- (31) Jiang, X.; Xiong, Q.; Nam, S.; Qian, F.; Li, Y.; Lieber, C. M. InAs/InP Radial Nanowire Heterostructures as High Electron Mobility Devices. *Nano Lett.* **2007**, *7* (10), 3214–3218. <https://doi.org/10.1021/nl072024a>.
- (32) Tilburg, J. W. W. van; Algra, R. E.; Immink, W. G. G.; Verheijen, M.; Bakkers, E. P. A. M.; Kouwenhoven, L. P. Surface Passivated InAs/InP Core/Shell Nanowires. *Semicond. Sci. Technol.* **2010**, *25* (2), 024011. <https://doi.org/10.1088/0268-1242/25/2/024011>.
- (33) Zhang, Y., Wu, J., Aagesen, M., Holm, J., Hatch, S., Tang, M., Huo, S.; Liu, H. Self-catalyzed ternary core–shell GaAsP nanowire arrays grown on patterned Si substrates by molecular beam epitaxy. *Nano letters*, 2014, *14*(8), 4542-4547. <https://doi.org/10.1021/nl501565b>
- (34) Lee, J. H.; Pin, M. W.; Choi, S. J.; Jo, M. H.; Shin, J. C.; Hong, S.-G.; Lee, S. M.; Cho, B.; Ahn, S. J.; Song, N. W.; Yi, S.-H.; Kim, Y. H. Electromechanical Properties and Spontaneous Response of the Current in InAsP Nanowires. *Nano Lett.* **2016**, *16* (11), 6738–6745. <https://doi.org/10.1021/acs.nanolett.6b02155>.
- (35) Shin, J. C.; Lee, A.; Katal Mohseni, P.; Kim, D. Y.; Yu, L.; Kim, J. H.; Kim, H. J.; Choi, W. J.; Wasserman, D.; Choi, K. J.; Li, X. Wafer-Scale Production of Uniform InAs_{1-x}P_x Nanowire Array on Silicon for Heterogeneous Integration. *ACS Nano* **2013**, *7* (6), 5463–5471. <https://doi.org/10.1021/nn4014774>.
- (36) Torres, C. M. S.; Stradling, R. A. Far Infrared Magneto-Optics of InAs_{1-x}P_x alloys under Hydrostatic Pressure. *Semicond. Sci. Technol.* 1987, *2* (6), 323–328. <https://doi.org/10.1088/0268-1242/2/6/001>.
- (37) Sourribes, M. J. L.; Isakov, I.; Panfilova, M.; Liu, H.; Warburton, P. A. Mobility Enhancement by Sb-Mediated Minimisation of Stacking Fault Density in InAs Nanowires Grown on Silicon. *Nano Lett.* **2014**, *14* (3), 1643–1650. <https://doi.org/10.1021/nl5001554>.
- (38) Belloeil, M.; Proietti, M. G.; Renevier, H.; Daudin, B. Nanoscale x-ray investigation of composition fluctuations in AlGaN nanowires. *Nanotechnology*, **2020**, *31*(37), 375709. <https://doi.org/10.1088/1361-6528/ab94e1>

-
- (39) Shiri, D.; Kong, Y.; Buin, A.; Anantram, M. P. Strain Induced Change of Bandgap and Effective Mass in Silicon Nanowires. *Appl. Phys. Lett.* **2008**, *93* (7), 073114.
<https://doi.org/10.1063/1.2973208>.
- (40) Wei, B.; Zheng, K.; Ji, Y.; Zhang, Y.; Zhang, Z.; Han, X. Size-Dependent Bandgap Modulation of ZnO Nanowires by Tensile Strain. *Nano Lett.* **2012**, *12* (9), 4595–4599.
<https://doi.org/10.1021/nl301897q>.
- (41) Zhang, Y., Fonseka, H. A., Aagesen, M., Gott, J. A., Sanchez, A. M., Wu, J., Kim, D.; Jurczak, P.; Huo, S.; Liu, H. Growth of pure zinc-blende GaAs (P) core–shell nanowires with highly regular morphology. *Nano letters*, **2017**, *17*(8), 4946-4950.
- (42) Joyce, H. J.; Boland, J. L.; Davies, C. L.; Baig, S. A.; Johnston, M. B. A Review of the Electrical Properties of Semiconductor Nanowires: Insights Gained from Terahertz Conductivity Spectroscopy. *Semicond. Sci. Technol.* **2016**, *31* (10), 103003.
<https://doi.org/10.1088/0268-1242/31/10/103003>.